

Multiple Photoluminescence from Pyrene-Fused Hexaarylbenzenes with Aggregation Enhanced Emission Features

Chuan-Zeng Wang,^[a] Yuki Noda,^[a] Chong Wu,^[a] Xing Feng,^{*,[b]} Perumal Venkatesan,^[c] Hang Cong,^[d] Mark R.J. Elsegood,^[e] Thomas G. Warwick,^[e] Simon J. Teat,^[f] Carl Redshaw,^[g] and Takehiko Yamato^{*,[a]}

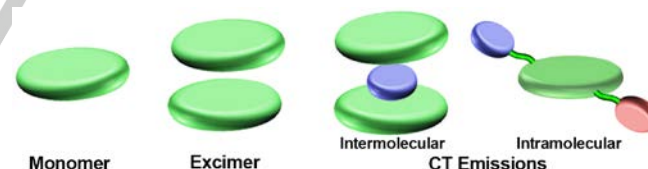
Abstract: Multiple photoluminescence, involved in monomer emission, excimer emission and charge transfer emission origin from new pyrene-fused hexaarylbenzenes (HAB) compounds were observed, which were designed and synthesized (in high yield) via the Diels-Alder reaction of bis(2-*tert*-butylpyren-6-yl)acetylene and tetraphenylcyclopentadienone. Although the distinction of between two molecules arises only from the geometrical position of one of the pyrenes, the NMR spectra, the crystal packing and the physicochemical properties of these pyrene-based HAB hybrids are distinctly different both in their solution state and in aggregation-state. The X-ray diffraction analysis clearly indicated that the pyrene moieties in this system would form different crystal packing in crystal state that can induce a fantastic multiple photoluminescence phenomenon.

Introduction

The construction of intriguing molecular structures is both an art and a science and has attracted considerable interest in recent years. Highlights include reports on cage-carborane-based dyads with aryl-substitution,¹ propeller-shaped tetraphenylethene-based aggregation-induced emission (AIE) luminogens with bulky pendant moieties,² chiral helicenes with fused planar and nonplanar systems,³ and π -expanded fullerene-based dyads.⁴ Such systems have played a crucial role

in developing the field of organic optoelectronics. Among the many promising hybrid candidates, hexaarylbenzene (HAB) appears to be an ideal scaffold given that it possesses a rigid core and adjustable aryl units, allowing for the formation of unusual and fascinating structures. It has also proved possible to extend the range of applications possible for HAB derivatives by the introduction of suitable radial substitution reactions.⁵

Pyrenes as typical polycyclic aromatic hydrocarbons (PAHs) possess unique optoelectronic properties and features that can be readily modified, which have allowed them to be extensively explored as fluorophores, particularly in view of their additional favorable stability and high fluorescence efficiency.⁶ Generally, the availability of efficient monomeric emission in the range of 370–430 nm and the excimer emission at around 480 nm,⁷ combined with the charge-transfer (CT) emission possible by means of the introduction of donor/acceptor moieties at the pyrene has established their position/reputation in comparison with other polyaromatic fluorophores (see examples in Scheme 1).⁸ However, the mechanisms associated with multiple photoluminescence from a single molecule in pyrene chemistry remains relatively unexplored. The minimal mechanistic work to-date reflects the limiting harsh prerequisites, such as the combination of multidimensional intermolecular interactions required, not to mention the pre-determined spatial arrangements combined with appropriate donor/acceptor constituents.⁹ Thus, the design and synthesis of organic molecules with multiple photoluminescence remains a challenging topic.



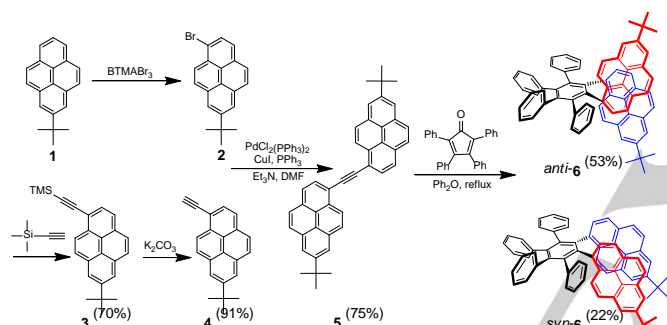
Scheme 1 Diagrammatic sketch illustrating the typical structures giving rise to emissions in the pyrene system.

Building on the individual emission mechanisms mentioned above, a new strategy to construct high-performance single molecules with multiple photoluminescence was conceived. Our target was to attempt to integrate a pyrene fluorophore with a propeller-shaped HAB scaffold into a single molecule, which would exhibit multiple photoluminescence, due to its multidimensional geometrical parameters, conformations and intra/inter-molecular interactions. In particular, we wished to construct this “propeller” by replacing two of the “propeller blades”. Herein, the synthesis of two conformers of the pyrene based HAB derivatives *anti*-6 and *syn*-6 was achieved by employing this molecular design. Fortunately, via diffusion of methanol vapor into a chloroform solution of each compound, single crystals were cultivated, and the intriguing structures of *anti*-6 and *syn*-6 are disclosed by X-ray crystallography (Fig. 1).

- [a] C.-Z. Wang, Y. Noda, Prof. T. Yamato
Department of Applied Chemistry, Faculty of Science and Engineering, Saga University
Honjo-machi 1, Saga 840-8502 (Japan)
E-mail: yamatot@cc.saga-u.ac.jp
- [b] Dr. X. Feng
Faculty of Material and Energy Engineering, Guangdong University of Technology, Guangzhou 510006, China.
E-mail: hyxhn@sina.com
- [c] Dr. P. Venkatesan
Lab. de Polimeros, Centro de Química, Instituto de Ciencias, Benemérita Universidad Autónoma de Puebla, Complejo de Ciencias, ICUAP, Edif. 103H, 22 Sur y San Claudio, Puebla, Puebla C.P. 72570, México
- [d] Prof. H. Cong,
Guizhou University, Guiyang 550025, China
- [e] Dr. M. R.J. Elsegood, Mr. T. G. Warwick
Chemistry Department, Loughborough University,
Loughborough, LE11 3TU, UK
- [f] Dr. S. J. Teat
ALS, Berkeley Lab, 1 Cyclotron Road, Berkeley, CA 94720, USA
- [g] Prof. C. Redshaw
Department of Chemistry, The University of Hull,
Cottingham Road, Hull, Yorkshire HU6 7RX, UK
Supporting information for this article is given via a link at the end of the document. *(Please delete this text if not appropriate)*

Results and Discussion

As depicted in Scheme 2, the bis(2-*tert*-butylpyren-6-yl)acetylene **5** was synthesized via the Sonogashira coupling reaction of 1-bromo-7-*tert*-butylpyrene **2** with 7-*tert*-butyl-1-ethynylpyrene **4** in 75% yield. 1,2-Bis(7-*tert*-butyl-pyren-1-yl)-3,4,5,6-(tetraphenyl)benzenes (*anti*-**6** and *syn*-**6**) were prepared by the Diels-Alder reaction of bis(2-*tert*-butylpyren-6-yl)acetylene **5** with 2,3,4,5-tetraphenylcyclopenta-2,4-dienone in one step (see ESI† for full synthetic procedures and characterisation data). These two stereoisomers could be cleanly separated by normal silica gel chromatography and recrystallization, affording *anti*-**6** as a pale green solid and *syn*-**6** as a yellow solid in 53% and 22% yields, respectively. The ^1H / ^{13}C NMR spectra, X-ray crystallography and HRMS clearly indicate that they are different compounds. Both compounds exhibited excellent thermal stability with decomposition temperatures (T_d) of 411 °C for *anti*-**6**, and 403 °C for *syn*-**6** under a nitrogen atmosphere at a heating rate of 10 °C min^{-1} , as shown in Table 1 and Supporting Information Fig. S11. Moreover, their fundamental photophysical properties and mechanism were investigated, which demonstrates the validity for the construction of multiple photoluminescence molecules utilizing this strategy.



Scheme 2 Synthetic route to *anti*-**6** and *syn*-**6**. TMS = trimethylsilyl.

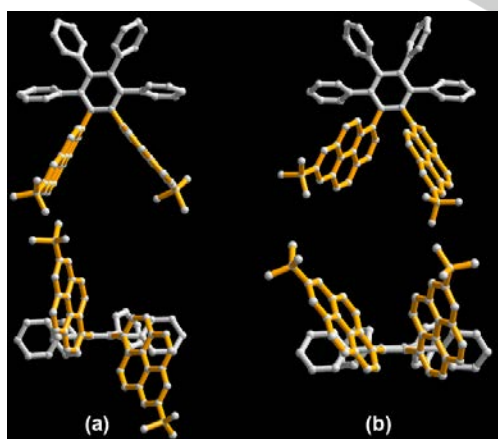


Fig. 1 The top (top) and side (bottom) views of the crystal structures of a) *anti*-**6**; b) *syn*-**6**. All the hydrogen atoms are omitted for clarity.

Analysis of the ^1H NMR spectra revealed well-resolved proton signals which could clearly distinguish these two isomers (see Fig. 2). As expected, for *anti*-**6**, six doublets (due to *ortho* coupling) (12H) and two singlets (4H) were observed for the pyrene moieties, though there is an overlap between one singlet (c' , $\delta_{\text{H}} = 8.02$ ppm) and one doublet (d' , $\delta_{\text{H}} = 8.01$ ppm). In comparison, the proton signals of *syn*-**6** exhibited a compact distribution, especially for the hydrogen atoms at the K-region of the pyrene moieties (d, e, f, g, 8H $\delta_{\text{H}} = 7.58$ – 7.70 ppm). In addition, the protons at the 6, 8-positions of pyrene completely overlap into one singlet (b, 4H, $\delta_{\text{H}} = 7.89$ ppm), reflecting the shielding effects induced by the spatial overlap of the aromatic rings. In addition, the thermostability and photochemical stability were further studied by ^1H NMR (Fig. S12), the interconversions of *anti*-**6** and *syn*-**6** was not observed after heating (lasted 30 min at 180 °C) and irradiation by UV light under air. The NMR spectrum indicated the isomer of *anti*-**6** and *syn*-**6** are remarkable conformational stability with of unique optical properties.

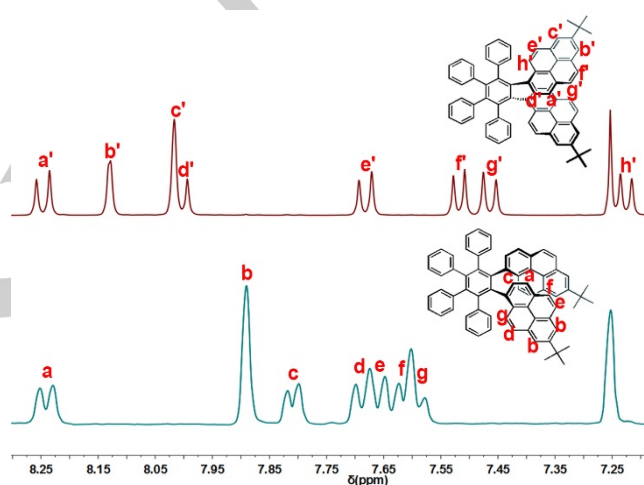


Fig. 2 Partial ^1H NMR spectra (400 MHz, 25 °C, CDCl_3) of *anti*-**6** (top) and *syn*-**6** (bottom).

The UV/Vis and photoluminescence (PL) spectra of *anti*-**6** and *syn*-**6** were investigated in dilute THF solution. Both compounds present multiple bands of different shapes in solution, which differ markedly from that of conventional pyrene-based chromophores (Fig. 3 left). *Anti*-**6** exhibited three weak, structureless absorptions for the $^1\text{L}_b$ bands at 403 nm ($\log \epsilon_{\text{max}} = 2.87 \text{ M}^{-1}\text{cm}^{-1}$), 353nm ($\log \epsilon_{\text{max}} = 4.72 \text{ M}^{-1}\text{cm}^{-1}$), and 283 nm ($\log \epsilon_{\text{max}} = 4.67 \text{ M}^{-1}\text{cm}^{-1}$), which correspond to $\text{S}_1 \leftarrow \text{S}_0$, $\text{S}_2 \leftarrow \text{S}_0$, and $\text{S}_3 \leftarrow \text{S}_0$, respectively, and are associated with the vibrational fine structure. Due to our experimental conditions, the $\text{S}_4 \leftarrow \text{S}_0$ transition band in the near ultraviolet region cannot be clearly assigned, which may originate from the nature of the pyrene structure.¹¹ *Syn*-**6** presents similar absorption properties. The details of the photophysical properties of the two stereoisomers are summarized in Table 1.

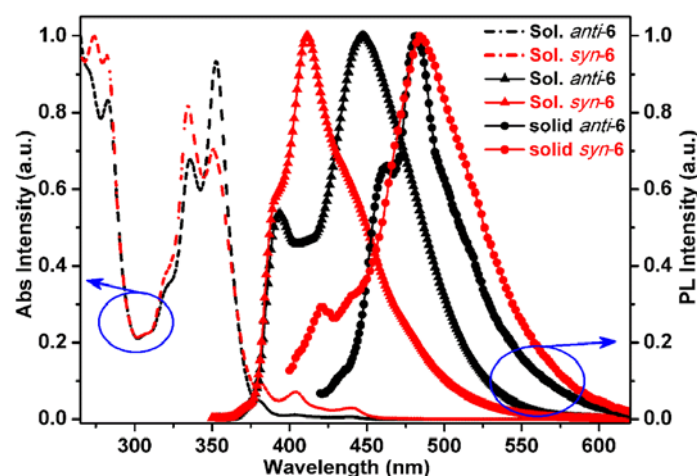


Fig. 3 UV/Vis absorption in THF solution, and fluorescence spectra of *anti-6* and *syn-6* in THF solution and in the solid state

Table 1 The photophysical properties of HAB derivatives *anti-6* and *syn-6*.

Py-based HAB	transition	λ_{Abs} [nm] ^[a] $\log \epsilon$, $\text{M}^{-1} \text{cm}^{-1}$	λ_{PL} [nm] ^[a]	λ_{PL} [nm] ^[b]	ϕ_{PL}		HOMO (eV)	LUMO (eV)	E_{g} (eV) ^[g]	
					Sol. ^[a]	Solid ^[b]				
<i>Anti-6</i>	$S_1 \leftarrow S_0$	403	2.87							
	$S_2 \leftarrow S_0$	353	4.72	394, 447	463, 482	0.60 (0%) ^[c] 0.95 (60%)	0.45	-5.01 ^[d] -5.32 ^[e]	-1.28 ^[d] -1.81 ^[f]	3.73 ^[g] 3.29 ^[g]
	$S_3 \leftarrow S_0$	283	4.67							
<i>Syn-6</i>	$S_1 \leftarrow S_0$	404	3.62							
	$S_2 \leftarrow S_0$	334	4.68	412	420, 484	0.46 (0%) 0.80 (60%)	0.10	-4.98 -5.25	-1.33 -1.72	3.65 3.28
	$S_3 \leftarrow S_0$	272	4.76							

[a] Measured in THF at room temperature. [b] Measured as powder. [c] the different fraction water in mixed solvents of THF and water are shown in bracket. [d] DFT (B3LYP/6-31G*) calculations were carried out with the use of structures optimized at the B3LYP/6-31G* level of theory. [e] Measured from the oxidation potential in THF solution by cyclic voltammetry. [f] LUMO = E_{g} + HOMO, [g] Estimated from the absorption edge of UV-Vis spectra.

In contrast to their similar absorption spectra, the stereoisomers *anti-6* and *syn-6* exhibited distinct emission bands in solution and in the solid state due to the different molecular conformations. Specifically, *anti-6* emitted blue light with two well-separated emission bands at 394 nm and 447 nm in THF solution. Based on our knowledge, the shoulder peak at 394 nm can be assigned to the monomeric emission of the pyrene-like chromophore,⁷ and the maximum peak at 447 nm can be attributed to the intermolecular interactions in this propeller-shaped multiple conjugated system. Similarly, *syn-6* also presents a blue emission band centred at 412 nm in THF solution (Fig. 3 right). Interestingly, new subsidiary peaks in both stereoisomers appeared in the solid state, which may indicate different molecular conformations are present leading to different emission behavior when compared with those observed in solution. As shown in Fig. 3, *anti-6* displays a red-shifted maximum emission peak at 482 nm with a shoulder peak at 463 nm, but no obvious emission band at 394 nm. It is reasonable to speculate that the new peak at 482 nm arises from the excimer emission and the shoulder peak at 463 nm may originate from a significant intermolecular interaction. We speculate that there is an intermolecular charge transfer (InterCT)¹² state resulting in the slight red-shift from the primary peak at 447 nm in solution to the subsidiary peak at 463 nm in the solid state. Also, similar optical characteristics were investigated for *syn-6*. In this system, it is easy to assign the monomeric emission and excimer

emission in solution and in the solid state from the multiple photoluminescence spectra. Taking *anti-6* as an example, we assumed that the emission band at 447 nm in solution and 463 nm in the solid state can be attributed to the InterCT emission. Given the polarity of the solution can exert slight effects on the CT emission, a solvatochromism experiment was carried out to provide further evidence. As shown in Fig. S13, *anti-6* exhibited a slight red-shift from the less polar cyclohexane (442 nm) to the more polar DMF (453 nm), while there is no obvious regularity with the increase of the polarity for the low wavelength emission band at around 394 nm. It further demonstrated that there is no intramolecular charge transfer (ICT) but InterCT for the *anti-6* system. Unsurprisingly, there is barely a change in the solvatochromism for *syn-6*. This is consistent with our conjecture and with the emission properties both in solution and in the solid state. Thus, the spectroscopic data strongly support the presence of multiple photoluminescence from the monomeric emission, excimer emission and CT emission in this system.

More detailed information on the multiple photoluminescence and its dependency on the molecular conformation can be gleaned from single crystal X-ray diffraction analysis of both stereoisomers.

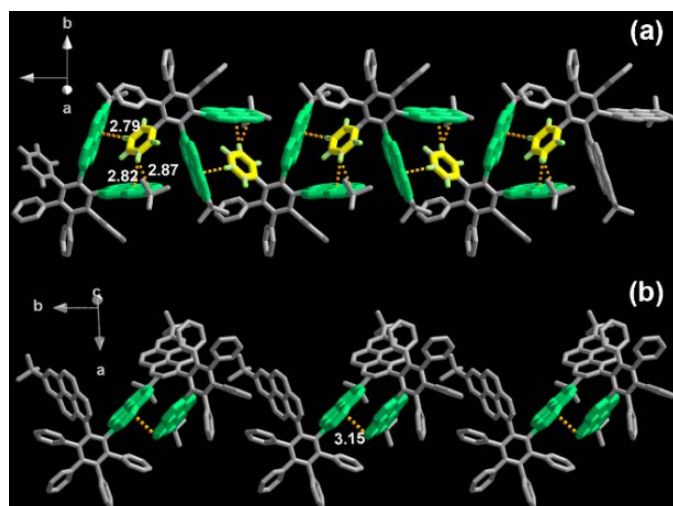


Fig. 4 The packing structures of compounds *anti-6* (a) and *syn-6* (b) with principal intermolecular packing interactions (most hydrogen atoms are omitted for clarity). Distances are in Å.

As is well known, the propeller-shaped HAB scaffold has proved to be a natural attraction due to its rigid hub and adjustable peripheries. The peripheral groups of the HAB scaffold generally undergo interlocking to exhibit interesting structural variations with fascinating photophysical properties. Hence, we further attempted to interpret the mechanism on the basis of the X-ray crystallographic results. Close inspection reveals that the HAB derivatives *anti-6* and *syn-6* present distinctively different spatial arrangements to each other. As shown in Fig. 4, a shell-like intermolecular donor-acceptor system was observed for *anti-6*, which was achieved by utilizing the electron-rich pyrene molecules as the donor “shell”, and the electron-deficient phenyl moieties as the acceptor “pearl”. The fragments comprising pyrene-phenyl-pyrene were present with displaced face-to-face patterns linked via C-H... π interactions with distances ranging from 2.79 to 2.87 Å. The pyrene moieties are almost mutually perpendicular. The formation of a donor-acceptor system is preferred to the formation of a charge transfer system. More interestingly, an obvious InterCT was observed and demonstrated via experimental and crystallographic studies, and the maximum InterCT emission was observed at 447 nm in THF solution. In contrast to *anti-6*, a clear pyrene...pyrene π ... π stacking interaction with a distance of 3.15 Å was observed in the packing of *syn-6*. Obviously, the π ... π stacking interaction plays a dominant role to affect the emission. The most direct evidence is that the excimer emission peak located at 484 nm appeared in the solid state, but was not observed in solution. These results are explicit and provide powerful evidence for the emission phenomenon and mechanism.

In general, HAB homologues exhibit a pronounced AIE property. To further investigate the AIE properties of the title compounds, the PL spectra of *anti/syn-6* (5×10^{-7} M) were recorded in a water/THF mixture with differing water content (Fig. 5a). Taking *anti-6* as an example, interesting AEE behavior was observed compared with previous reports.¹³ In particular, on increasing the water fraction in the water/THF mixture from 0% to 60%, the emission intensity was enhanced by about 2-fold (solid line). This is due to the restricted intramolecular rotation (RIR) and led to enhanced emission in this propeller-shaped system.^{13c} However, when the content of water was increased

up to 99%, the emission gradually decreased and a new peak was observed compared with the original emission in THF solution (dashed line), which resulted from the formation of excimer and solvent polarity dependent InterCT emission.¹⁴ It is worth mentioning that the emission profiles present a coherent transition from the organic solution to the solvent mixtures, aggregates and solid state. In the pure organic phase, two

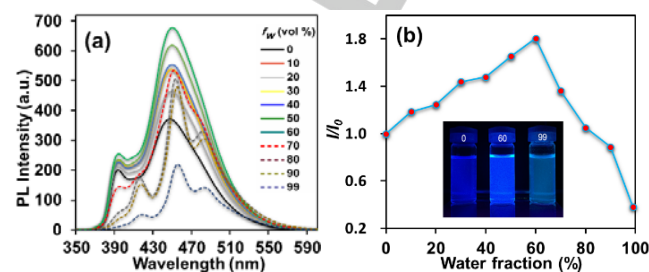


Fig. 5 a) PL spectra of *anti-6* in THF/H₂O mixtures (5×10^{-7} M). b) Plots of I/I_0 values versus the compositions of aqueous mixtures of *anti-6*.

well-separated emission bands were observed as monomeric emission (394 nm) and CT emission (447), and this type of emission band remains unaltered until the water percentages were increased up to 60%, inducing the formation of aggregation. Gradually, as the water fraction increased to more than 60%, multiple emission spectra gradually appeared, which are due to the monomeric emission (416 nm), CT emission (453 nm), and excimer formation (481), respectively. The PL spectra exhibited during the ultimate stage, suggested that excimer emission plays a dominant role and CT emission is secondary in the solid state. Similar AEE properties and transitions for the emission can also be observed for *syn-6* (Fig. S14). In case of *syn-6*, there are two main emissions, including monomeric (412 nm) and excimer emission (484 nm). In particular, it is worth mentioning that the concentration-dependent luminescence observed for the two compounds are in excellent agreement with the AEE properties (Figures S15–16). Increasing emission intensity is displayed on increasing the concentration until the luminescence reaches its maximum intensity, following which the luminescence decreases in intensity when the concentration is further increased; similar red-shifts and multiple photoluminescence were also observed in these results. Furthermore, the fluorescence quantum yields were measured in solution and in the solid state, and the quantum yields (ϕ_{PL}) are listed in Table 1. Specifically, a noticeable enhancement of quantum yield from 60% (in THF solution) to 95% (at 60% water fraction) was observed for *anti-6*, and a subdued quantum yield (45%) was obtained in the solid state, which is due to the formation of excimer. Similar optical behavior was observed in molecule *syn-6*.

To provide further evidence for the energy states, cyclic voltammetry (CV) and DFT calculations (B3LYP/6-31G*) were performed on *anti-6* and *syn-6* to interpret the electronic states combined with the photophysical properties. As shown in Fig. S18, both the compounds **6** displayed irreversible redox processes with distinct positive potentials in the vicinity of 1.4 V in solution. As shown in Figures S19–20, the electronic distributions of **6** in the ground state were further studied by frontier orbital analysis. As expected, both optimized geometries are consistent with their single crystal X-ray structures (Table S1). In order to derive explicit evidence, Time-dependent DFT (TD-DFT) calculations were carried out with the program

package Gaussian at the B3LYP/6-31G* level of theory. Simulated electronic spectra were produced based on the TD-DFT results, which are largely consistent with the experimental results. The TD-DFT calculations show that the pyrene moiety plays a dominant role on the orbital transition to the electronic excitation according to the respective contributions. In this system, the stronger $S_4 \leftarrow S_0$ transition is described by a near 50:50 contribution from HOMO-1 \rightarrow LUMO+1 and HOMO-1 \rightarrow LUMO of the shoulder absorption band of *anti*-**6**, so these three key frontier molecular orbitals should be considered in any discussion of this system. Specifically, the shoulder absorption is due to the different combination of HOMO-1 \rightarrow LUMO+1 and HOMO-1 \rightarrow LUMO with a very high oscillator strength ($f = 0.416$, and $f = 0.289$), and the low oscillator strengths of 0.078 for $S_n \leftarrow S_0$ ($n = 1, 2, 3$), respectively. These theoretical results provided further insight into the intensity of the absorption spectra shown in Fig. 3. The detailed results of the TD-DFT calculations for the ground-state optimized geometries for *anti*-**6** and *syn*-**6** are presented in the Supporting Information, along with simulated absorption spectra.

Conclusions

In summary, by utilizing a propeller-shaped HAB scaffold, we have observed intriguing multiple photoluminescence. In particular, the thermally stable *anti*-**6** and *syn*-**6** pyrene-fused hexaarylbenzenes synthesized herein exhibit unusual AEE characteristics. Multiple emission mechanisms, including monomer, excimer and CT emission were explored and deciphered in a single molecule. Single crystal X-ray structures of these two compounds **6** provided further insight into their differing properties. It is envisioned that the present work will widen our thinking in photophysics and stimulate work on innovative light-based technologies.

Experimental Section

General procedures

Synthetic routes for the two compounds *anti*-**6** and *syn*-**6** are shown in Scheme 2. All reactions were carried out under a dry argon atmosphere. Solvents were Guaranteed reagent (GR) for cyclohexane, 1,4-dioxane, tetrahydrofuran (THF), dichloromethane (CH_2Cl_2), and dimethylformamide (DMF), and stored over molecular sieves. Other reagents were obtained commercially and used without further purification. Reactions were monitored using thin layer chromatography (TLC). Commercial TLC plates (Merck Co.) were developed and the spots were identified under UV light at 254 and 365 nm. Column chromatography was performed on silica gel 60 (0.063–0.200 mm). All synthesized compounds were characterized using $^1\text{H-NMR}$, $^{13}\text{C-NMR}$ spectroscopy, and HRMS (FAB) mass analysis and target compounds were characterized by synchrotron X-ray crystallography.

Synthesis of 7-*tert*-butyl-1-(trimethylsilylethynyl)pyrene (**3**)

To a stirred solution of 7-*tert*-butyl-1-bromopyrene **2**¹⁰ (1.40 g, 4.15 mmol), Et_3N (20 mL) and THF (20 mL), was added trimethylsilylacetylene (1.17 mL, 8.30 mmol) and PPh_3 (65.3 mg, 0.249 mmol), and the mixture was stirred at room temperature under argon. $\text{PdCl}_2(\text{PPh}_3)_2$ (87.2 mg, 0.125 mmol), CuI (23.6 mg, 0.125 mmol) were then added, and the mixture was heated to 80 °C with stirring for 24 h. After it was cooled, the mixture was diluted into CH_2Cl_2 (200 mL) and washed successively with saturated aqueous NH_4Cl , H_2O and brine. The organics were dried (MgSO_4), and the solvents were evaporated. In order to obtain pure product, the crude product was purified twice by column chromatography, eluting with hexane/ CHCl_3 (9:1), and recrystallized from methanol to afford the desired compound **3** as a light green solid (1.03 g, 70%). M.p. 163–164 °C; $^1\text{H-NMR}$ (300 MHz, CDCl_3): $\delta_{\text{H}} = 0.39$ (s, 9H, TMS), 1.59 (s,

9H, *t*Bu), 7.98–8.16 (m, 5H, pyrene-*H*), 8.23 (s, 1H, pyrene-*H*), 8.25 (s, 1H, pyrene-*H*), 8.53 ppm (d, $J = 9.0$ Hz, 1H, pyrene-*H*); $^{13}\text{C-NMR}$ (100 MHz, CDCl_3): $\delta_{\text{C}} = 31.92, 35.27, 99.99, 104.22, 117.35, 122.51, 122.90, 122.92, 124.17, 124.29, 125.41, 127.09, 128.43, 128.60, 129.63, 130.90, 131.06, 131.23, 132.10, 149.42$ ppm; FAB-MS: m/z calcd for $\text{C}_{25}\text{H}_{26}\text{Si}$ 354.18 [M^+]; found 354.17 [M^+]; anal. calcd (%) for $\text{C}_{25}\text{H}_{26}\text{Si}$ (354.56): C 84.69, H 7.39, Si 7.92; found: C 84.86, H 7.21.

Synthesis of 7-*tert*-butyl-1-ethynylpyrene (**4**)

To a stirred solution of 7-*tert*-butyl-1-(trimethylsilylethynyl)pyrene **3** (1.00 g, 2.82 mmol) and THF (20 mL), was added MeOH (20 mL) and K_2CO_3 (585 mg, 4.23 mmol). The reaction was stirred at room temperature for 12 h. The mixture was quenched by addition of a large amount of water, extracted with dichloromethane (2×50 mL), washed with water and dried over anhydrous MgSO_4 and concentrated. The residue obtained was recrystallized in methanol to obtain 7-*tert*-butyl-1-ethynylpyrene **4** (728 mg, 91%) as light green needles. M.p. 119–120 °C; $^1\text{H-NMR}$ (300 MHz, CDCl_3): $\delta_{\text{H}} = 1.59$ (s, 9H, *t*Bu), 3.61 (s, 1H, $-\text{C}\equiv\text{CH}$), 8.01 (d, $J = 8.9$ Hz, 1H, pyrene-*H*), 8.05–8.17 (m, 4H, pyrene-*H*), 8.24 (s, 1H, pyrene-*H*), 8.26 (s, 1H, pyrene-*H*), 8.56 ppm (d, $J = 9.2$ Hz, 1H, pyrene-*H*); $^{13}\text{C-NMR}$ (100 MHz, CDCl_3): $\delta_{\text{C}} = 31.91, 35.27, 82.41, 82.88, 116.24, 122.45, 122.99, 123.02, 124.17, 124.27, 125.17, 127.04, 128.62, 128.77, 129.82, 130.86, 131.03, 131.44, 132.34, 149.51$ ppm; FAB-MS: m/z calcd for $\text{C}_{22}\text{H}_{18}$ 282.14 [M^+]; found 282.14 [M^+]; anal. calcd (%) for $\text{C}_{22}\text{H}_{18}$ (282.38): C 93.57, H 6.43; found: C 93.39, H 6.52.

Synthesis of bis(2-*tert*-butylpyren-6-yl)acetylene (**5**)

To a stirred solution of 7-*tert*-butyl-1-bromopyrene **2** (500 mg, 1.48 mmol), Et_3N (20 mL) and DMF (20 mL), was added 7-*tert*-butyl-1-ethynylpyrene **4** (503 mg, 1.78 mmol) and PPh_3 (62.2 mg, 0.237 mmol), and the mixture was stirred at room temperature under argon. $\text{PdCl}_2(\text{PPh}_3)_2$ (72.8 mg, 0.104 mmol) and CuI (31.1 mg, 0.163 mmol) were then added, and the mixture was heated to 100 °C with stirring for 24 h. After it was cooled, the mixture was diluted into CH_2Cl_2 (200 mL) and washed successively with saturated aqueous NH_4Cl , H_2O and brine. The organics were dried (MgSO_4), and the solvents were evaporated. In order to obtain pure product, the crude product was purified twice by column chromatography, eluting with hexane/ CHCl_3 (3:7), and recrystallized from hexane/dichloromethane (8:2, v/v) to afford the desired compound **5** as an orange solid (599 mg, 75%). M.p. 345–347 °C; $^1\text{H-NMR}$ (300 MHz, CDCl_3): $\delta_{\text{H}} = 1.61$ (s, 18H, *t*Bu), 8.05 (d, $J = 8.8$ Hz, 2H, pyrene-*H*), 8.11 (d, $J = 8.8$ Hz, 2H, pyrene-*H*), 8.17 (d, $J = 8.0$ Hz, 2H, pyrene-*H*), 8.23–8.29 (m, 6H, pyrene-*H*), 8.36 (d, $J = 8.0$ Hz, 2H, pyrene-*H*), 8.86 ppm (d, $J = 9.2$ Hz, 2H, pyrene-*H*); $^{13}\text{C-NMR}$ (100 MHz, CDCl_3): $\delta_{\text{C}} = 31.93, 35.28, 94.46, 117.92, 122.66, 122.95, 124.46, 124.55, 125.59, 127.16, 128.40, 128.70, 129.51, 131.01, 131.17, 131.76, 149.48$ ppm; FAB-MS: m/z calcd for $\text{C}_{42}\text{H}_{34}$ 538.27 [M^+]; found 538.25 [M^+]; anal. calcd (%) for $\text{C}_{42}\text{H}_{34}$ (282.38): C 93.64, H 6.36; found: C 93.56, H 6.42.

Synthesis of 1,2-bis(7-*tert*-butyl-pyren-1-yl)-3,4,5,6-(tetraphenyl)benzenes (**6**)

Compound **5** (100 mg, 0.279 mmol) and 2,3,4,5-tetraphenylcyclopenta-2,4-dienone (161 mg, 0.419 mmol) were dissolved in Ph_2O (2.0 mL) under argon. The mixture was refluxed for 24 h and then the solvent was removed *in vacuo*. The residue was subjected to column chromatography on silica gel (CH_2Cl_2 /hexane 4:6) to afford *anti*-**6** (88.8 mg, 53%) as a pale-green solid and *syn*-**6** (36.1 mg, 22%) as a yellow solid. *anti*-**6**: M.p. >400 °C; $^1\text{H-NMR}$ (400 MHz, CDCl_3): $\delta_{\text{H}} = 1.54$ (s, 18H, *t*Bu), 6.37–6.48 (m, 4H, Ph-*H*), 6.61 (t, $J = 7.5$ Hz, 2H, Ph-*H*), 6.78 (d, $J = 7.1$ Hz, 2H, Ph-*H*), 6.86–7.01 (m, 12H, Ph-*H*), 7.22 (d, $J = 7.9$ Hz, 2H, pyrene-*H*), 7.46 (d, $J = 9.0$ Hz, 2H, pyrene-*H*), 7.52 (d, $J = 7.9$ Hz, 2H, pyrene-*H*), 7.68 (d, $J = 9.0$ Hz, 2H, pyrene-*H*), 8.00 (d, $J = 9.2$ Hz, 2H, pyrene-*H*), 8.02 (s, 2H, pyrene-*H*), 8.13 (d, $J = 1.7$ Hz, 2H, pyrene-*H*), 8.24 ppm (d, $J = 9.2$ Hz, 2H, pyrene-*H*); $^{13}\text{C-NMR}$ (100 MHz, CDCl_3): $\delta_{\text{C}} = 31.92, 35.11, 121.63, 121.80, 122.69, 123.16, 123.65, 125.14, 125.25, 125.94, 126.33, 126.42, 126.62, 127.28, 128.09, 128.81, 129.12, 130.45, 130.62, 130.87, 131.00, 131.50, 131.71, 135.94, 139.92, 140.05, 140.64, 140.82, 141.66, 148.43$ ppm; FAB-HRMS (MALDI-TOF): m/z calcd for $\text{C}_{70}\text{H}_{54}$ 894.4226 [M^+]; found 894.4423 [M^+]. *syn*-**6**: M.p. 214–215 °C; $^1\text{H-NMR}$ (400 MHz, CDCl_3): $\delta_{\text{H}} = 1.42$ (s, 18H, *t*Bu), 6.36–6.46 (m, 4H, Ph-*H*), 6.57 (t, $J = 7.4$ Hz, 2H, Ph-*H*), 6.83–6.94 (m, 12H, Ph-*H*), 7.10 (d, $J = 7.5$ Hz, 2H, Ph-*H*), 7.58 (d, $J = 8.6$ Hz, 2H, pyrene-*H*), 7.61 (d, $J = 7.5$ Hz, 2H, pyrene-*H*),

7.66 (d, $J = 8.8$ Hz, 2H, pyrene-*H*), 7.68 (d, $J = 9.2$ Hz, 2H, pyrene-*H*), 7.80 (d, $J = 7.9$ Hz, 2H, pyrene-*H*), 7.89 (s, 4H, pyrene-*H*), 8.23 ppm (d, $J = 9.2$ Hz, 2H, pyrene-*H*); ^{13}C NMR (100 MHz, CDCl_3): $\delta_{\text{C}} = 31.81, 34.97, 121.56, 122.61, 122.70, 123.77, 125.10, 125.23, 125.97, 126.26, 126.54, 126.60, 126.63, 126.78, 127.01, 128.88, 129.14, 129.92, 130.48, 130.58, 130.71, 130.81, 131.49, 131.65, 135.69, 140.12, 140.25, 140.71, 140.87, 141.96, 148.09$ ppm; FAB-HRMS (MALDI-TOF): m/z calcd for $\text{C}_{70}\text{H}_{54}$ 894.4426 [M^+]; found 894.4418 [M^+].

Acknowledgements

This present work was performed under the Cooperative Research Program of "Network Joint Research Center for Materials and Devices (Institute for Materials Chemistry and Engineering, Kyushu University)". We would like to thank the National Science Foundation of China (No. 21602014), Fund Program for the Scientific Activities of Selected Returned Overseas Professionals of Beijing, the OTEC at Saga University and the International Cooperation Projects of Guizhou Province (No. 20137002) for financial support and the EPSRC for an overseas travel grant to C.R. The Advanced Light Source is supported by the Director, Office of Science, Office of Basic Energy Sciences, of the U.S. Department of Energy under Contract No. DE-AC02-05CH11231.

Keywords: Multiple Photoluminescence • Hexaarylbenzenes • Pyrene Chemistry • Anti/Syn Conformations • Aggregation Enhanced Emission

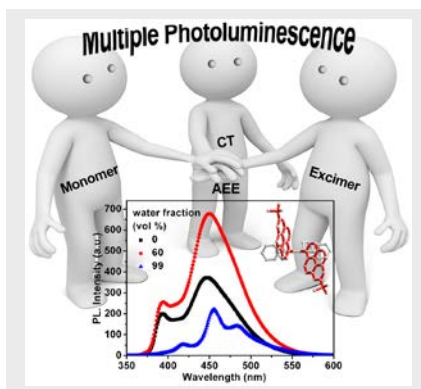
- [1] a) K.-R. Wee, W.-S. Han, D. W. Cho, S. Kwon, C. Pac, S. O. Kang, *Angew. Chem., Int. Ed.* **2012**, *51*, 2677–2680; b) K.-R. Wee, Y.-J. Cho, J. K. Song, S. O. Kang, *Angew. Chem., Int. Ed.* **2013**, *52*, 9682–9685.
- [2] a) P. I. Shih, C. Y. Chuang, C. H. Chien, E. W. G. Diau, C. F. Shu, *Adv. Funct. Mater.* **2007**, *17*, 3141–3146; b) Z. Zhao, P. Lu, J. W. Y. Lam, Z. Zhang, C. Y. K. Chan, H. H. Y. Sung, I. D. Williams, Y. Ma, B. Z. Tang, *Chem. Sci.* **2011**, *2*, 672–675; c) Z. Zhao, S. Chen, C. Y. K. Chan, J. W. Y. Lam, C. K. W. Jim, P. Lu, Z. Chang, H. S. Kwok, H. Qiu, B. Z. Tang, *Chem. – Asian J.* **2012**, *7*, 484–488; d) Z. Zhao, S. Chen, J. W. Y. Lam, P. Lu, Y. Zhong, K. S. Wong, H. S. Kwok, B. Z. Tang, *Chem. Commun.* **2010**, *46*, 2221–2223.
- [3] a) M. Gingras, *Chem. Soc. Rev.* **2013**, *42*, 968–1006; b) T. Fujikawa, Y. Segawa, K. Itami, *J. Am. Chem. Soc.* **2015**, *137*, 7763–7768; c) T. Fujikawa, Y. Segawa, K. Itami, *J. Am. Chem. Soc.* **2016**, *138*, 3587–3595.
- [4] a) L. Sánchez, R. Otero, J. M. Gallego, R. Miranda, N. Martín, *Chem. Rev.* **2009**, *109*, 2081–2091; c) P. Moreno-García, A. L. Rosa, V. Kolivoška, D. Bermejo, W. J. Hong, K. Yoshida, M. Baghernejad, S. Filippone, P. Broekmann, T. Wandlowski, N. Martín, *J. Am. Chem. Soc.* **2015**, *137*, 2318–2327.
- [5] a) R. R. Hu, J. W. Y. Lam, Y. Liu, X. Zhang, B. Z. Tang, *Chem. Eur. J.* **2013**, *19*, 5617–5624; b) V. Vij, V. Bhalla, M. Kumar, *Chem. Rev.* **2016**, *116*, 9565–9627; c) D. Lungerich, D. Reger, H. Hölzel, R. Riedel, M. J. C. Martin, F. Hampel, N. Jux, *Angew. Chem., Int. Ed.* **2016**, *55*, 5602–5605.
- [6] a) T. M. Figueira-Duarte, K. Müllen, *Chem. Rev.* **2011**, *111*, 7260–7314; b) X. Feng, J. Y. Hu, C. Redshaw, T. Yamato, *Chem. –Eur. J.* **2016**, *22*, 11898–11916.
- [7] D. A. Safin, M. G. Babashkina, M. P. Mitoraj, P. Kubisiak, K. Robeyns, M. Bolte, Y. Garcia, *Inorg. Chem. Front.* **2016**, *3*, 1419–1431.
- [8] a) T. Förster, *Angew. Chem., Int. Ed.* **1969**, *8*, 333–343; b) A. Ueno, I. Suzuki, T. Osa, *J. Am. Chem. Soc.* **1989**, *111*, 6391–6397; c) B. Zhao, N. Li, X. Wang, Z. Chang, X. H. Bu, *ACS Appl. Mater. Interfaces* **2017**, *9*, 2662–2668; d) C. Z. Wang, H. Ichiyang, K. Sakaguchi, X. Feng, M. R. J. Elsegood, C. Redshaw, T. Yamato, *J. Org. Chem.* **2017**, *82*, 7176–7182.
- [9] H. J. Ju, K. Wang, J. Zhang, H. Geng, Z. T. Liu, G. X. Zhang, Y. S. Zhao, D. Q. Zhang, *Chem. Mater.* **2017**, *29*, 3580–3588.
- [10] X. Feng, J. Y. Hu, H. Tomiyasu, Z. Tao, C. Redshaw, M. R. J. Elsegood, L. Horsburgh, S. J. Teat, X. F. Wei, T. Yamato, *RSC Adv.* **2015**, *5*, 8835–8848.
- [11] A. G. Crawford, A. D. Dwyer, Z. Q. Liu, A. Steffen, A. Beeby, L.-O. Palsson, D. J. Tozer, T. B. Marder, *J. Am. Chem. Soc.* **2011**, *133*, 13349–13362.
- [12] L. J. Sun, W. G. Zhu, W. Wang, F. X. Yang, C. C. Zhang, S. F. Wang, X. T. Zhang, R. J. Li, H. L. Dong, W. P. Hu, *Angew. Chem., Int. Ed.* **2017**, *56*, 7831–7835.
- [13] a) Z. K. Wang, J. Y. Nie, W. Qin, Q. L. Hu and B. Z. Tang, *Nat. Commun.* **2016**, *7*, 12033; b) G. Singh, S. I. Reja, V. Bhalla, D. Kaur, P. Kaur, S. Arora, M. Kumar, *Sens. Actuators B* **2017**, *249*, 311–320; c) J. Mei, N. L. C. Leung, R. T. K. Kwok, J. W. Y. Lam, B. Z. Tang, *Chem. Rev.* **2015**, *115*, 11718–11940.
- [14] a) H. Li, Z. Chi, X. Zhang, B. Xu, S. Liu, Y. Zhang, J. Xu, *Chem. Commun.* **2011**, *47*, 11273–11275; b) T. Jadhav, B. Dhokale, Y. Patil, S. M. Mobin, R. Misra, *J. Phys. Chem. C* **2016**, *120*, 24030–24040.

Entry for the Table of Contents (Please choose one layout)

Layout 1:

FULL PAPER

Text for Table of Contents



Chuan-Zeng Wang, Yuki Noda, Chong Wu, Xing Feng,* Perumal Venkatesan Hang Cong, Mark R.J. Elsegood, Thomas G. Warwick, Simon J. Teat, Carl Redshaw, and Takehiko Yamato*

Page xx – Page xx

Multiple Photoluminescence from Pyrene-Fused Hexaarylbenzenes with Aggregation Enhanced Emission Features